# Geometric issues in reverse osmosis: numerical simulation and experimentation

G. Srivathsan, Ephraim Sparrow and John Gorman

## ABSTRACT

This investigation is a synergistic combination of laboratory experimentation and numerical simulation to quantify the practical impact of geometric imperfections in the flow channels of a reverse osmosis (RO) system. To this end, carefully executed experiments are performed to quantify the fluid flow in a system containing feed spacers which are embedded in the RO membrane. In a complementary activity, numerical simulations were performed both for an ideal geometric situation (without embedments) and the actual geometric configuration including the embedments. It was found that the presence of unaccounted embedments affected the pressure drop predictions for the system by 14–19%. When account was taken of the embedments, the simulation results were found to be virtually coincident with the experimental results. This outcome suggests that deviations between experimental and simulation results encountered in the literature might well have been due to geometrical deviations of the type investigated here. The numerical simulation of the feedwater fluid flow was based on the often-used but unverified assumption that the velocity field experiences the geometric periodicity of the feed spacer. This assumption was lent support by results from a non-periodic simulation model and by the excellent agreement between the numerically based predictions and the experimental data.

**Key words** | experiments, feed spacer embedment, flow-passage dimensions, numerical simulation, reverse osmosis

**G. Srivathsan**
**Ephraim Sparrow** (corresponding author)
**John Gorman**
Department of Mechanical Engineering,
University of Minnesota, Minneapolis,
Minnesota, 55455,
USA
E-mail: *esparrow@umn.edu*

## INTRODUCTION

There is a pressing need for reducing the energy consumption needed for the implementation of the reverse osmosis (RO) system for processing non-potable water. The design of such systems is based on a rich literature containing both numerical simulation and experimentation. The status of the information reported in the open literature has been aptly chronicled by Fimbres-Weihs & Wiley (2010) and by Johnson & Busch (2010). From the first of these reviews, it is evident that the majority of the work is based on computational fluid dynamics (CFD). The second review traces the qualitative history of the evolution of RO systems and their components. One of the observations conveyed by Johnson & Busch (2010) is that feed spacers may be deeply embedded into the RO membrane. The quantitative impact of this situation remains undetermined, and one of the foci of this work is to determine its importance.

One of the focus issues of CFD modeling is the widespread use of a feedwater flow model based on the periodic geometry of the flow passage. This geometric periodicity motivated the adoption of a streamwise-periodic model of the fluid flow, and Darcovich *et al.* (2009), Fimbres-Weihs & Wiley (2007), Koutsou *et al.* (2004, 2007), Lau *et al.* (2009), Li *et al.* (2002, 2005), Ranade & Kumar (2006) and Shakaib *et al.* (2007, 2009) are representative of the literature related to this model. Some reservations have been expressed about the validity of the streamwise-periodic fluid-mechanic model, but it appears that the quantitative implications of the model have not yet been assessed. Such an assessment is a second focus of this investigation.

A comparison of numerically predicted and experimentally determined flow-passage pressure drop was displayed in Fimbres-Weihs & Wiley (2010). Although it was concluded there that good agreement prevailed, that conclusion may have been based on the commonality of the trends. A careful assessment requires consideration of

doi: 10.2166/wst.2014.367

the logarithmic scale, from which deviations as large as a factor of two were observed.

The present research is a synergistic involvement of numerical simulation and laboratory experimentation. The experiments were performed with extreme care and attention to detail with the aspiration of establishing a high standard of quality. The experimental apparatus was precisely modeled by the numerical simulation, thereby enabling a valid comparison to be made between the results extracted from the two approaches. This comparison led to a means for explaining the reasons for the differences between simulation and experimental results.

## EXPERIMENTATION

### Experimental facility

A schematic diagram of the experimental apparatus is displayed in Figure 1. The description of the setup is facilitated by following the path of fluid flow starting with the feedwater pump. Pressurized working fluid is delivered by a variable-speed feedwater pump (a) to a micro-porous filter (b) from which it passes through a feedwater temperature and pH management system (c). This system is capable of automatically maintaining the pH and the temperature of the feedwater at preselected experimental conditions. The default condition used for the measured results is 25 °C and the pH of 8. The feed pressure of the fluid entering the RO modules (e) is measured by the master feedwater pressure gauge (d). An RO module consists of an assemblage of RO pressure vessels connected in series. Each pressure vessel houses a commercially available 6.35 cm (2.5 inch) diameter and 1 m long RO element. Pressures are measured at each end of the six pressure vessels by means of pressure transducers (f) whose resolution is 70 Pa (0.01 psi). The pressure drop across each element is thereby determined. The high-pressure working fluid exiting the RO modules (e) is throttled by a pressure-regulating valve (g). The flow rate of the feedwater is measured by an electronic flow rate measuring device (h) before the feedwater is collected in the feedwater tank for recirculation. The resolution of this flow rate measuring device is 0.0631 $cm^3/s$ (0.001 gpm).

A schematic diagram of an RO pressure vessel is displayed in Figure 2, The use of an experimental facility involving multiple pressure vessels was chosen to provide redundancy for the sake of more accurate results. For the same reason, replicate data runs for each of nine Reynolds numbers were performed four separate times over a period of 4 days (see Table S1 in the Appendix, available online at http://www.iwaponline.com/wst/070/367.pdf).

Feed spacers with 0.072 cm (0.028 inch) thickness and seven strands per 2.54 cm (1 inch) with a 90° strand angle were used in the experiments. The elements were tested

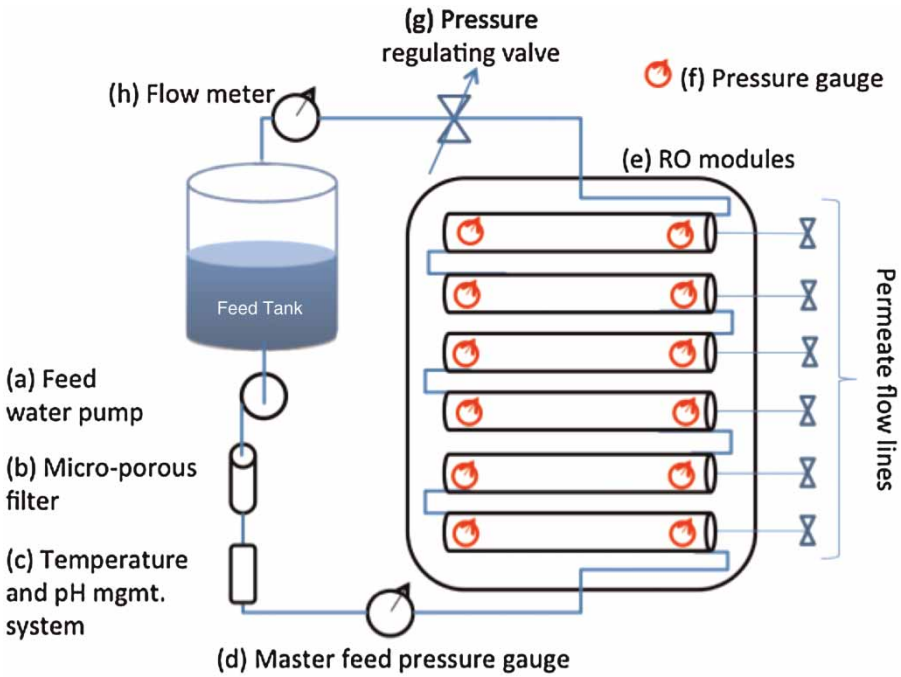


**Figure 1** | Schematic diagram of the experimental facility.

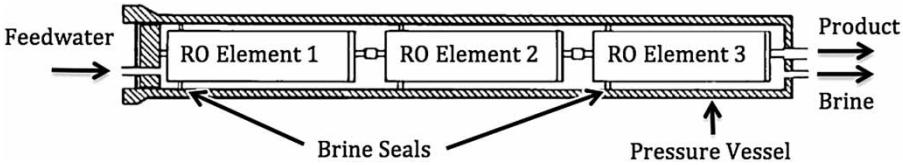


**Figure 2** | Schematic diagram of an RO pressure vessel.

for defects, damages, and leaks prior to their use. After loading the RO elements into their pressure vessels, the system was flushed with soft water to remove any preservatives. The working fluid for the experiments was surrogate feedwater synthesized by mixing pure water (e.g., product water from an RO system) and common salt (1,000 ppm by weight). This mixture had a salinity equal to 1 g/kg.

### Experimental procedure

Although the test facility could be operated to produce product water, this function was disabled because it did not add to the focus of the experiment, which was to determine the relationship between pressure drop and feedwater flow rate. In the implementation of the experiments, the flow rate of the feedwater passing through the feed spacer was controlled, and the corresponding per-element pressure drop was measured by the aforementioned transducers. The flow rate through the RO elements was controlled by setting the speed of the positive displacement pump. The temperature of the system was controlled and maintained at 25 °C.

In preparation for the experiments performed on a given day, the system was cleaned on the previous day by hydrochloric acid at pH of 2 for 30 minutes followed by sodium hydroxide (base) at pH of 13 for 30 minutes. The system was later neutralized and then flushed with RO product water at pH of 8 at 8 L/min overnight. The foregoing procedures were performed to ensure that no contaminants that could foul the system and alter the pressure drop data existed in the system during the experiment and data collection. The feedwater line has a micron filter and a carbon filter to prevent any fouling that may occur from accidental pollutants in the line.

As a precaution to avoid prejudicial occurrences such as non-standard elements taken from a particular batch, elements from different batches of the same stock-keeping unit (SKU) were systematically intermixed over the course of the experimental work. The Appendix (available online at http://www.iwaponline.com/wst/070/367.pdf) sets forth the Reynolds numbers of the respective data runs. The range of Reynolds numbers investigated was from approximately 100 to 800. Correspondingly, the flow rate was varied from approximately 63 to 630 $cm^3/s$ (1–10 gpm). All told, 34 data runs were performed with system cleaning imposed before each set of eight/nine runs.

The experimental results are presented after the following description of the numerical simulations.

## NUMERICAL SIMULATION

### Physical model

Numerical simulation was performed as a precise counterpart of the experimentation described in the foregoing. Most commercial RO elements use non-woven fibers as feed spacers. To ensure congruence of the experimental and computational models, non-woven feed spacer fibers were adopted for the simulation. This selection ensures the validity of comparisons between the predictions of the simulation and the experimental data. Figure 3(a) illustrates the nature of a non-woven feed spacer, whereas Figure 3(b) shows an array of spacers. Only 90° strand angles are considered here as well as two-layer-strand symmetric spacers because they are the most common type of feed spacer utilized in most commercial RO elements. The direction of flow is parallel to the bisector of the angle formed by the two-strand-layer configuration. As can be seen from the figure, the spacer thickness is approximately equal to twice the strand diameter since the two strands are stacked one atop the other. In this investigation, the strand angle is

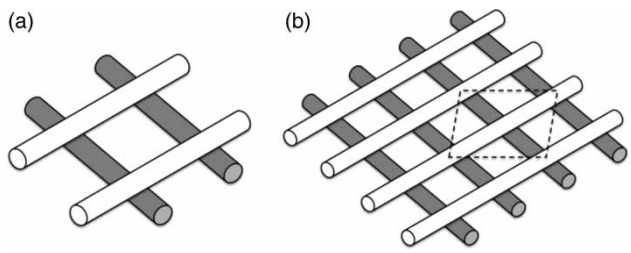


**Figure 3** | Illustrations of non-woven feed spacers. (a) A single pair of spacers and (b) an array of spacers (the box shows the 'repeating unit' used for CFD simulation).

maintained constant at 90°, and the strand spacing and the spacer thickness are varied.

Spatially periodic boundary conditions are used on all four sides of the feed spacer, a model which will be justified in detail shortly. The geometry of the adopted strand configuration is displayed in Figure 3(b), and the dimensions of the adopted feed spacers are given in Table 1. The geometric factor of the feed spacer is the ratio of the feed spacer thickness to the distance between two feed spacer strands.

## Numerical analysis

At the outset of the simulation work, the issues of flow regime (laminar vs. turbulent) and temporal state (steady vs. unsteady) were investigated. It was found from computational experiments that for the operating conditions relevant to practice, a model based on laminar steady flow was appropriate. Since the flowing medium has a salinity of 1 g/kg, its viscosity and density are indistinguishable from those of pure water. Furthermore, inasmuch as the temperature is constant, the participating fluid properties (density and viscosity) can be regarded as constant. As a consequence, the flow is governed by the three-dimensional Navier–Stokes equations supplemented by the equation of continuity. These equations are, respectively,

$$\rho\left(u_i\frac{\partial u_j}{\partial x_i}\right) = -\frac{\partial p}{\partial x_j} + \frac{\partial}{\partial x_i}\left(\mu\frac{\partial u_j}{\partial x_i}\right) \; j = 1, 2, 3 \tag{1}$$

$$\frac{\partial u_i}{\partial x_i} = 0 \tag{2}$$

In these equations, $\rho$ and $\mu$ denote the density and viscosity of the fluid. The quantity $u_i$ is the velocity component in the $i$-direction, and $x_i$ is the coordinate in the $i$-direction; the pressure is $p$.

The boundary conditions which govern the solutions of these equations have to be carefully considered. As written, the foregoing equations appear to require two independent boundary conditions in each of the three coordinate directions. However, in this regard, reference to Figure 3(b) indicates that the 'geometry' is symmetric in the transverse direction and is spatially periodic in the direction of fluid flow. This observation suggests that a periodic solution for the fluid flow in the mainflow direction might be possible. The existence of a spatially periodic fluid flow solution depends on the nature of the interaction between the fluid and its bounding walls. The bounding walls are, in fact, the surfaces of the membrane. In actual practice, product water passes through the surfaces of the membrane, and strictly speaking, this reality negates a spatially periodic solution. In the past, other investigators have assumed that a periodic solution is admissible without justification. In what follows, a logical rationalization will be presented.

The essence of a spatially periodic solution is the recognition that the flow field repeats without modification from one geometrically similar module to the next. This pattern of fluid flow means that the velocity distribution at the inlet face of each module must be identical to the velocity distribution at the exit face of that module. A necessary condition for this to occur is that the mass flow rate at the inlet and exit faces be identical. However, as noted in the foregoing, there is an outflow of product water through the membrane wall, which diminishes the mass flow rate in the mainflow direction.

To assess the impact of the departure from strict periodicity, an approach was adopted as follows. First, a periodic model was implemented, and the velocity distribution at the inlet (and the exit) of the periodic module was extracted. Then, a non-periodic model was formulated in which the velocity distribution extracted from the periodic model was imposed at the inlet of a module whose geometry is the same as that for the periodic case. However, at the downstream end of the module, periodicity was not applied. Instead, a very weak 'opening' boundary condition was utilized. In the parlance of numerical simulation, an opening condition allows the fluid crossing the boundary in question to have complete freedom to find its own direction. As a consequence, the solution based on this model does not require identical velocity distributions at inlet and exit. In recognition of the outflow of the product water, a value for the velocity passing perpendicular to the surface of the membrane was imposed. That value, 0.00002 m/s, was based on a realistic estimate from practice.

For the non-periodic solution, the change in the velocity between the inlet and exit faces of the module in

**Table 1** | Dimensions of the adopted feed spacers in mils (1 mil = 0.0254 mm)

| Feed spacer | Spacer thickness | Distance between strands | Strand radius | Geometric factor |
|---|---|---|---|---|
| 1 | 20 | 100 | 5.71 | 0.2 |
| 2 | 25 | 100 | 7.14 | 0.25 |
| 3 | 30 | 100 | 8.57 | 0.3 |
| 4 | 35 | 100 | 10 | 0.35 |

question was 0.145%. Given a typical velocity in the main-flow direction of 0.15 m/s, the reduced velocity at outflow would be 0.1498 m/s. This insignificant change serves to validate the spatially periodic model used in the numerical simulations. A further validation is provided by Figure 4. This figure displays a pair of color contour diagrams for the velocity. Figure 4(a) corresponds to the solution based on spatial periodicity, while Figure 4(b) is for the non-periodic solution. These two diagrams appear to be identical in every respect.

A careful study was made to establish the accuracy of the numerical simulations. In this regard, a mesh independence evaluation was performed. A typical outcome of this study is a change in the dimensionless pressure drop of 0.5% when the number of elements was increased from 1,140,000 to 9,050,000. To perform the numerical simulation, ANSYS CFX 14.0 finite-volume software was used.

## RESULTS AND DISCUSSION

Two distinct sets of numerical simulations were performed. For the first set, the dimensions of the flow channel were those provided by the manufacturer of the RO elements. The motivation for the second set of simulations was the discovery that the feed spacers were deeply embedded into the RO membrane. This observation supports a similar finding reported by Johnson & Busch (2010). The impact of the deep embedment of the feed spacers into the membrane is that the dimensions of the passage for feedwater flow are reduced with respect to the indicated dimensions. This reduction in cross-sectional area leads to higher feedwater flow velocities relative to those based on the ideal feed spacer geometry.

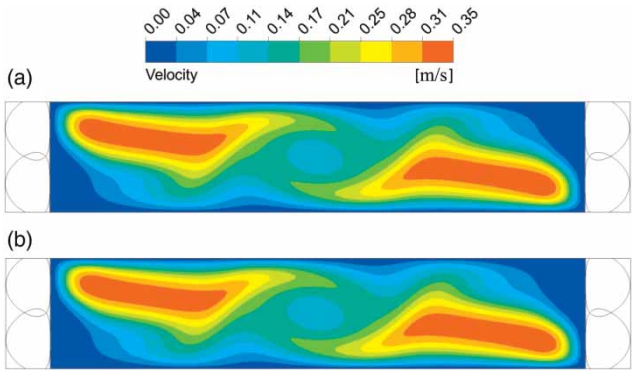


**Figure 4** | Comparison of velocity color contour diagrams comparing the periodic and non-periodic solutions.

Two sets of comparisons will be made here, respectively based on the numerical solutions for the original geometry and on the revised geometry. Both comparisons bring together the numerical predictions for each geometry and the experimental data. To facilitate the comparison of results, it is appropriate to use dimensionless groupings. The pressure results were expressed in terms of the friction factor $f$ defined as

$$f = \frac{\left(-\frac{dp}{dx}\right) D_h}{\frac{1}{2}\rho U^2} \tag{3}$$

In this equation, the pressure gradient $(-dp/dx)$ was determined as the ratio of the pressure drop across the element divided by the length of the element. The hydraulic diameter, $D_h$, is twice the feed spacer thickness, $U$ is the actual bulk velocity of the feed flow in the feed spacer, and $\rho$ is the fluid density. The friction factor will be presented as a function of the Reynolds number, $Re$, of the feed spacer flow, whose definition is

$$Re = \frac{\rho U D_h}{\mu} \tag{4}$$

The fluid viscosity is represented by $\mu$.

Table S1 in the Appendix (available online at http://www.iwaponline.com/wst/070/367.pdf) shows the experimentally observed friction factor for various Reynolds numbers.

A comparison will now be made between the numerical predictions based on the manufacturer-indicated

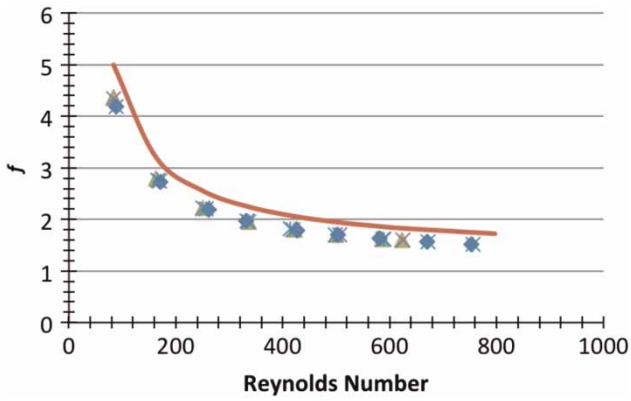


**Figure 5** | Comparison of the numerical predictions, based on the manufacturer-indicated dimensions of the flow passage, with the experimental data. The predictions are represented by the continuous curve and the experiments by the discrete points.

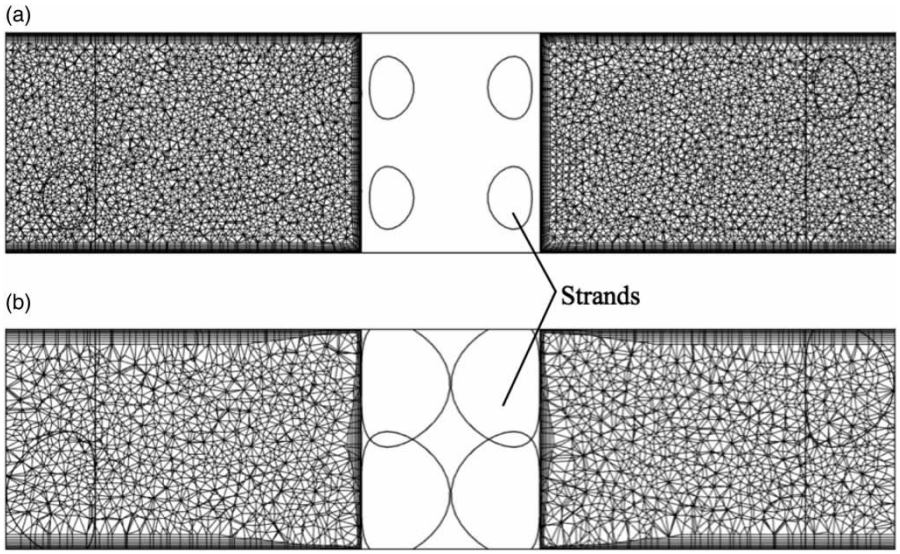


**Figure 6** | Meshes for the geometries based on (a) manufacturer's specifications and (b) actual intruded geometry.

dimensions of the flow channel and the experimental data. This information is conveyed in Figure 5. In addition to the curve that represents the predictions, the figure contains experimental data which were replicated several times to assure their accuracy. From the figure, it is seen that the trend displayed by the data is reproduced by the trend of the predictions. The predictions fall in the range from 14 to 19% above the data.

Subsequent to the discovery of the feed spacer embedment within the RO membrane, the actual dimensions of the flow passage were carefully reassessed and used as input for the next set of numerical simulations. In this regard, the meshing of the solution domain had to be revised to take into account the actual dimensions associated with the feed spacer embedment. The meshes for the geometry corresponding to the manufacturer-indicated dimensions and that for the actual intruded geometry are displayed in Figures 6(a) and (b), respectively. It can be seen from the diagrams that the strands have been pushed together due to the intrusion of the feed spacer embedment.

The comparison of the newly simulated results and the experimental data is set forth in Figure 7. Inspection of the figure reveals excellent agreement between the results of the numerical predictions and the experimental data. This outcome indicates the necessity of knowing accurate dimensions of the flow passage as a perquisite for any numerical simulation undertaking.

It is worthy of note that the numerical simulations of Figures 5 and 7 correspond to appropriately different

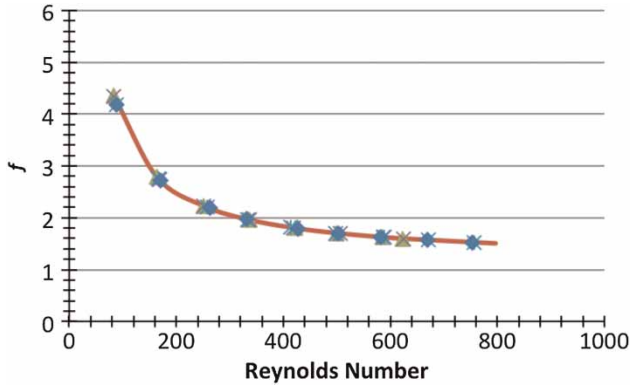


**Figure 7** | Comparison of the numerical predictions, based on the measured dimensions of the flow passage, with the experimental data. The predictions are represented by the continuous curve and the experiments by the discrete points.

geometries. The geometry on which Figure 5 is based is that whose dimensions correspond to the manufacturer's specifications. On the other hand, the simulation results conveyed in Figure 7 were obtained using the actual intruded geometry of the feed spacer used in the experiments.

The lack of quantitative recognition of the possible feed spacer embedment in the RO membrane during membrane fabrication may well have influenced previous comparisons between numerical predictions and experimental data. During the manufacturing of the spiral-wound membrane, the spiral stack is tied (wound) by applying mechanical force. This force acts on the feed spacer–membrane

interface and leads to the embedment of the feed spacer into the RO membrane.

## CONCLUDING REMARKS

The research described here is a synergistic approach to the modeling of the RO system of water purification that includes both experimentation and numerical simulation. The special strength of the work is the geometrical fidelity maintained between the experimental and computational models.

The initial simulation was developed by making use of dimensions supplied by the manufacturer of the RO elements that were utilized in the experiments. The friction factors (dimensionless pressure drops) extracted from the simulations were compared with those determined experimentally. The comparison showed that both sets of results displayed a similar trend as a function of the Reynolds number. However, the predictions lay from 14 to 19% above the data.

Based on a qualitative observation in the literature (Johnson & Busch 2010), this outcome motivated a very careful assessment of the actual dimensions of the element's flow passages. A complete disassembly revealed that the feed spacers were deeply embedded into the RO membrane, so that the actual flow-passage dimensions were smaller than those based on the manufacturer's specifications.

When new simulations were performed making use of the actual flow-passage dimensions, excellent agreement was found to exist between the experimental and numerical results.

Literature comparisons between simulation and experimental results have typically displayed deviations. On the basis of the present experience, it may be conjectured that those deviations could possibly be due to dimensional differences between the simulation and experimental models. An understanding of the manufacturing of the RO element and the subsequent magnitude of feed spacer embedment into the RO membrane is necessary to create an accurate CFD geometry that will represent the actual dimensions of the feed spacer installed in an RO element. Any work performed in simulating the flow of feedwater through the feed spacer of a spiral-wound RO element would yield deviating results unless the feed spacer embedment phenomenon is understood.

The numerical simulation of the feedwater fluid flow was based on the often-used assumption that the velocity field is in step with the geometric periodicity of the feed spacer. However, seemingly for the first time, this assumption was given a logical underpinning.

## REFERENCES

Darcovich, K., Dal-Cin, M. M. & Gros, B. 2009 Membrane mass transport modeling with periodic boundary condition. *Comput. Chem. Eng.* **33**, 213–224.

Fimbres-Weihs, G. A. & Wiley, D. E. 2007 Numerical study of mass transfer in three-dimensional spacer-filled narrow channels with steady flow. *J. Membr. Sci.* **306**, 228–243.

Fimbres-Weihs, G. A. & Wiley, D. E. 2010 Review of 3D CFD modeling of flow and mass transfer in narrow spacer-filled channels in membrane modules. *Chem. Eng. Process.* **49**, 759–781.

Johnson, J. & Busch, M. 2010 Engineering aspects of reverse osmosis module design. *Desal. Water Treat.* **15**, 236–248.

Koutsou, C. P., Yiantsios, S. G. & Karabelas, A. J. 2004 Numerical simulation of the flow in plane channel containing a periodic array of cylindrical turbulence promoters. *J. Membr. Sci.* **231**, 81–90.

Koutsou, C. P., Yiantsios, S. G. & Karabelas, A. J. 2007 Direct numerical simulation of flow in spacer-filled channels: effect of spacer geometrical characteristics. *J. Membr. Sci.* **291**, 53–69.

Lau, K. K., Abu Baker, M. Z., Ahmad, A. L. & Murugesan, T. 2009 Feed spacer mesh angle, 3D modeling, simulation and optimization based on unsteady hydrodynamics in spiral wound membrane channel. *J. Membr. Sci.* **343**, 16–33.

Li, F., Meindersma, W., de Haan, A. B. & Reith, T. 2002 Optimization of commercial net spacers in spiral wound membranes modules. *J. Membr. Sci.* **208**, 289–302.

Li, F., Meindersma, W., de Haan, A. B. & Reith, T. 2005 Novel spacers for mass transfer enhancement in membrane separations. *J. Membr. Sci.* **253**, 1–12.

Ranade, V. V. & Kumar, A. 2006 Fluid dynamics of spacer filled rectangular and curvilinear channels. *J. Membr. Sci.* **271**, 1–15.

Shakaib, M., Hasani, S. M. F. & Mahmood, M. 2007 Study on the effects of spacer geometry in membrane feed channels using three-dimensional computational flow modeling. *J. Membr. Sci.* **297**, 74–89.

Shakaib, M., Hasani, S. M. F. & Mahmood, M. 2009 CFD modeling for flow and mass transfer in spacer-obstructed membrane feed channels. *J. Membr. Sci.* **326**, 270–284.

First received 17 December 2013; accepted in revised form 11 August 2014. Available online 5 September 2014